3D luminescent concentrators

P. Pichon, François Balembois, Frédéric Druon, Patrick Georges

Research Article Vol. 29, No. 5 / 1 March 2021 / Optics Express 6915
Optics EXPRESS

3D luminescent concentrators

PIERRE PICHON,* FRANÇOIS BALEMBOIS, FRÉDÉRIC DRUON, AND PATRICK GEORGES

Université Paris-Saclay, Institut d'Optique Graduate School, CNRS, Laboratoire Charles Fabry, 91127 Palaiseau, France
**pierre.pichon@institutoptique.fr*

Abstract: A solution to develop high-brightness incoherent sources consists in luminescent concentration. Indeed, the absorption/emission process in a high index medium allows us to circumvent the brightness conservation law by the confinement of the light in 1 or 2 dimensions. In practice, Ce-doped luminescent concentrators pumped with InGaN LED exceed LED's brightness by one order of magnitude. This work shows how light confinement in 3 dimensions increases the brightness by an additional order of magnitude. Thanks to an analytical approach validated by experimental results, this concept gives new degrees of freedom for the design of luminescent concentrators and paves the way to a generation of incoherent sources among the brightest ever designed.

1. Introduction

One can basically sort light sources in two categories: incoherent light sources which can deliver high powers with a limited brightness and coherent light sources which are able to deliver high brightness at limited powers. The brightness is intrinsically related to the emission process which is isotropic for incoherent sources (fluorescence, electroluminescence, thermal emission) or direction selective for lasers (stimulated emission) and synchrotrons (magnetobremsstrahlung radiation). Light sources combining power, brightness and incoherence are crucial for many applications relative to lighting and imaging but are challenging to design. Indeed, the use of laser is often prohibitive for lighting applications due to its coherence that generates speckle and reduces the image quality. The brightness of laser can be degraded to solve this problem either by diffusion [1], random lasing [2] or by secondary emission in phosphors [3]. However, these sources are power-limited compared to incoherent sources. Another approach consists in the design of higher brightness light sources based on the existing powerful incoherent sources. Light recycling [4] consists in the redirection of a part of the emitted light toward the emitters. Providing that the emitters are partially transparent or partially reflective, this redirected light can be added to the direct emission resulting in a brightness enhancement. This concept has been investigated for thermal emission in discharge lamps [5,6] with a radiance enhancement between 1.35 and 1.6. Likewise, spectral recycling of the infrared part of the spectrum of light bulbs with interference layers can improve the brightness in the visible by a factor 3 [7]. Light recycling has also been investigated with light emitting diodes (LED) using a specular or a diffuse reflector cup backscattering the light emitted by the phosphors LED layer [8]. The reflectivity of LEDs can even be used to build a reflective cavity consisting in LED walls closed by diffused reflective ends [9]. A brightness enhancement of 2 is reported when the output surface is partially closed by a mirror. A brightness enhancement of 1.7 has been measured as a result of LED light recycling inside a concentric parabolic concentrator having reflective edges [10]. It is worth to note that the brightness enhancement in lamps and LEDs is intrinsically limited by the absorption of the emitters : absorption of the plasma in arc lamps, absorption of the filament in light bulbs, absorption of the semi-conductor in LEDs. To go further with light recycling, one must choose emitting media with low losses. This is the case of luminescent concentrators (LC).

#415268 https://doi.org/10.1364/OE.415268
Journal © 2021 Received 30 Nov 2020; revised 4 Feb 2021; accepted 4 Feb 2021; published 19 Feb 2021

Optics EXPRESS

Known for fifty years, a luminescent solar concentrator (LSC) is a slab embedded with luminophores [11]. One of the large faces of the slab is exposed to the sun to pump the luminophores. The losses are small enough for the guided light to be efficiently collected at the four small edges of the slab with photovoltaic cells [12]. This configuration is well suited for large area panels for photovoltaic windows [13–15]. As a part of the light emitted by the luminophores is confined in 1-dimension by total internal reflections on two parallel faces, LSCs can be referred as 1D luminescent concentrators. The performance of LSCs is evaluated by the concentration factor defined as the ratio of the brightness of the edge faces versus the brightness of the sun on the ground. Typical concentration factors for LSCs are around ten [11].

Since the early 2010's, an extension of the concept of LC appeared with high power LEDs instead of the sun to pump the luminophores. Compared to LSCs, LED-pumped LC are light sources with a single output face (usually one of the smallest edge face). Hence, the light is collected along one propagation axis. As the useful light is confined in 2-dimensions by total internal reflections on the four faces parallel to the output axis, LED-pumped luminescent concentrators can be referred as 2D luminescent concentrators (2D-LCs). 2D-LCs have taken benefit from the maturity of InGaN LEDs developed for the lighting market and from the maturity of cerium-doped crystals developed for scintillators. A major asset of LED-pumped 2D-LCs is power scaling and massive collective operation: two thousand LEDs have been used for the pumping of a single Ce:YAG luminescent concentrator [16]. Ce:YAG crystals pumped by blue LEDs have produced high brightness emission in the yellow-orange (550–650 nm) for various applications such as medical lighting (2.3 W/mm^2/sr [17]), digital projection (1.1 W/mm^2/sr [18,19]) and solid state laser pumping (1.5 W/mm^2/sr [16] and 12 W/mm^2/sr [20] in quasi-continuous wave operation). To characterize LED-pumped 2D-LC, a concentration factor has been defined [16] as the output brightness over the brightness of a single pump LED. This concentration factor reaches 10 to 20 following the state of the art [16–20] and corresponds to the brightness enhancement compared to a single LED.

Spectral recycling by self-absorption in 2D-LC has been investigated in previous works [19]. The aim of this work is to push the concept of luminescent concentration one step further: the emitted light will be confined in three dimensions by total internal reflections on the 4 faces parallel to the output axis and by additional mirrors put on the faces perpendicular to the output axis. This setup will be referred to as 3D luminescent concentrators (3D-LC). This work presents a simple analytical approach of the concept comparing the brightness enhancement of a 3D-LC compared to a 2D-LC having the same dimensions. It gives the first experimental demonstration of 3D luminescent concentration on a Ce:YAG crystal uniformly illuminated.

2. Analytical approach of the concept of 3D concentration

2.1. Brightness of a 2D luminescent concentrator

The purpose of this section is to derive an analytical expression of the brightness of a 2D luminescent concentrator. It is characterized by a cuboid shape with its length, width and thickness respectively noted l, w and t (Fig. 1(a)). The six faces of the LC are optically polished and are denoted by their dimensions: faces l×t, w×l and w×t (Fig. 1(a)). This model assumes that the dimensions of the LC are set such that $l \geq w \geq t$ (limit case corresponding to a cube). The LC contains luminophores with a uniform density per unit volume noted n_t, each of them emitting a power φ_e at a given wavelength. The LC is characterized by a propagation loss coefficient α (cm^{-1}) at the emitted wavelength. The output face has a surface S = w×t. The face opposite to the output face is covered by a "back" mirror in order to recycle the light propagating towards this opposite face. This corresponds the usual configuration reported in the literature [16–20]. The refractive index of the LC is noted n and the LC is assumed to be surrounded by air.

Among the rays emitted in the concentrator, part are trapped inside the parallelepiped and part go through the 6 faces. In this approach, we consider only the rays that can be transmitted by

Optics EXPRESS

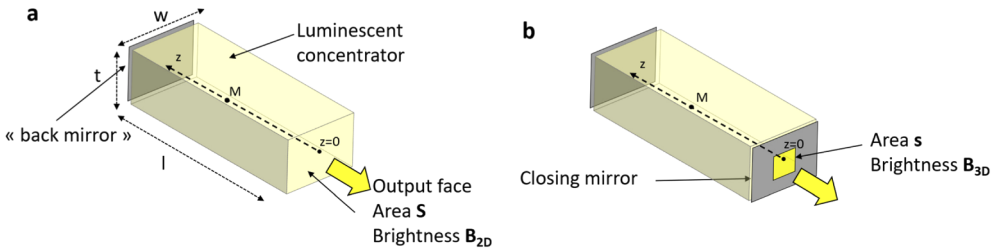

Fig. 1. Concept of the brightness enhancement with 3D luminescent concentrator. a, 2D luminescent concentrator. A HR mirror is added to the w×t back face. The output (front) face has an area S with a brightness B_{2D}. b, 3D luminescent concentrator. For brightness enhancement, the output face is partially closed by a mirror except on a small area s. B_{3D} is the brightness of the reduced output surface.

the output face and by the opposite face. The rays collected after the output surface are limited in angle of incidence, either by total internal reflection or by the optical system used to collect the rays outside the LC. The maximum angle inside the LC for the rays collected by this optical system is noted θ_{max}. Here, $\theta_{max} \leq \theta_{TIR}$ with $\sin(\theta_{TIR})=1/n$. The rays emitted inside the LC can be divided in two parts: the rays going directly toward the output surface, corresponding to a power P_1, and the rays reflected on the back mirror before reaching the output face (power P_2). The total output power collected just before the output surface is the sum of the powers: $P = P_1 + P_2$.

The angle θ_{max} define a bunch of rays inside the LC with a solid angle $2\pi(1\text{-}\cos(\theta_{max}))$. For a random emitting point M of coordinate z on the propagation axis (Fig. 1(a)), one can define an average propagation distance in the LC for the rays emitted directly to the output surface:

$$d(z) = -z\frac{\ln cos(\theta_{max})}{1-cos(\theta_{max})} \tag{1}$$

For n=1.83, corresponding to the refractive index of Ce:YAG used in this work, the maximum angle is $\theta_{TIR}=33°$ and the average path is $d(z) = 1.09\times z$, very close to the distance z between the point and the output surface. We assume, for the simplicity, that all the rays concerned propagate along this average distance d(z) before reaching the output face. In the following d(l) is noted d for simplicity. Each point of coordinate z emits the same amount of power towards the output face. Hence by integration over the crystal length l, the power P_1 related to the rays directly reaching the output surface is:

$$P_1 = \frac{\phi_e n_t S}{2\alpha \ln(cos(\theta_{max}))}(1 - cos(\theta_{max}))^2(e^{-\alpha d} - 1) \tag{2}$$

Because of Fresnel reflection, the power emitted by the output face $P_{2D,11}$ is:

$$P_{2D,11} = T_{Fresnel}P_1 \tag{3}$$

With $T_{Fresnel}$ the transmission of the output surface. Assuming small incidence angles, we approximate $T_{Fresnel} = 1 - \left(\frac{n-1}{n+1}\right)^2$ without polarization dependance.

A part of the power is recycled in the LC because of Fresnel reflections: $(1 - T_{Fresnel})P_1$. The corresponding rays come back to the output face after a reflection on the back mirror (R) and an average travel distance in the LC of 2d. Consequently, the output power after this second impact

Optics EXPRESS

on the output face is:

$$P_{2D,12} = T_{Fresnel} e^{-2\alpha d} R(1 - T_{Fresnel}) P_1 \tag{4}$$

The total output power $P_{2D,1tot}$ is the sum of all the powers transmitted by the output aperture after the multiple bounces:

$$P_{2D,1tot} = \sum_{k=1}^{\infty} P_{2D,1k} = P_1 \frac{T_{Fresnel}}{1-e^{-2\alpha d} R(1-T_{Fresnel})} \tag{5}$$

The rays from the point M reaching the output surface after reflection on the back mirror propagate over a longer average distance: d(2l-z). Taking the reflection coefficient of the back mirror in account, the power P_2 related to those rays is:

$$P_2 = R \frac{\phi_e n_i S}{2\alpha \ln(cos(\theta_{max}))} (1 - \cos(\theta_{max}))^2 e^{-2\alpha d} (1 - e^{\alpha d}) \tag{6}$$

Similarly, the contribution of the rays firstly reflected to the back mirror can be derived ($P_{2D,2tot}$). By summing all the power, the total power emitted by the output face is P_{2D}:

$$P_{2D} = P_{2D,1tot} + P_{2D,2tot} = (P_1 + P_2) \frac{T_{Fresnel}}{1-e^{-2\alpha d} R(1-T_{Fresnel})} \tag{7}$$

Let us define the maximal output angle after refraction at the output surface: θ'_{max}, such that:

$$n\ sin(\theta_{max}) = sin(\theta'_{max}) \tag{8}$$

The brightness B_{2D} of this 2D-LC averaged over the output solid angle is:

$$B_{2D} = \frac{P_{2D}}{2\pi S(1-\cos(\theta'_{max}))} \tag{9}$$

2.2. Brightness of a 3D luminescent concentrator

A second HR mirror of reflectivity R is added to partially cover the output face. The remaining uncovered portion of the face consists in an aperture (Fig. 1(b)). The light is now also partially confined in the dimension perpendicular to the output face. This confinement in 3 dimensions is referred as 3D-luminescent concentrators (3D-LC). The area of the aperture is noted s and we define the aperturing ratio r = S/s. Contrary to the previous case (2D-LC), many rays will be trapped by the additional mirror inside the LC and will undergo multiple additional bounces on the w×t faces before reaching the aperture.

Let us consider the rays propagating directly to the output face (corresponding to P_1 in the previous case). Assuming a homogeneous distribution of the rays inside the LC, a ray incident on the output face has a probability to go through the aperture given by the ratio of the surfaces: s/S=1/r. This means that the power incident on the aperture related to this first impact on the output surface is $\frac{1}{r}P_1$. Because of Fresnel reflection, the output power $P_{3D,11}$ is:

$$P_{3D,11} = \frac{T_{Fresnel}}{r} P_1 \tag{10}$$

The power recycled in the LC after this first impact is composed of two parts: $\left(1 - \frac{1}{r}\right) R\ P_1$ corresponding to a reflection probability on the mirror covering the output face and $\frac{1-T_{Fresnel}}{r} P_1$ corresponding to the Fresnel reflection on the aperture interface. The corresponding rays come

Optics EXPRESS

back to the output face after a reflection on the back mirror and an average travel distance in the LC of 2d. Consequently, the output power after the second impact on the output face is:

$$P_{3D,12} = \frac{T_{Fresnel}}{r} e^{-2\alpha d} \left[\frac{1-T_{Fresnel}}{r} R + \left(1 - \frac{1}{r}\right) R^2 \right] P_1 \tag{11}$$

The total output power $P_{3D,1tot}$ is the sum of all the powers that are incident on the output aperture:

$$P_{3D,1tot} = \sum_{k=1}^{\infty} P_{3D,1k} = \frac{T_{Fresnel}}{r} P_1 \frac{1}{1-e^{-2\alpha d}\left[\frac{1-T_{Fresnel}}{r} R + \left(1-\frac{1}{r}\right)R^2\right]} \tag{12}$$

The same method can be used to find the contribution of the rays firstly reflected to the back mirror (corresponding to P_2). By summing all the power, the total power incident on the output aperture is P_{3D}:

$$P_{3D} = P_{3D,1tot} + P_{3D,2tot} = \frac{1}{r}(P_1 + P_2) \frac{T_{Fresnel}}{1-e^{-2\alpha d}\left[\frac{1-T_{Fresnel}}{r} R + \left(1-\frac{1}{r}\right)R^2\right]} \tag{13}$$

The brightness of the output aperture, averaged over the output solid angle, is then given by:

$$B_{3D} = \frac{P_{3D}}{2\pi s(1-\cos(\theta'_{max}))} \tag{14}$$

2.3. Brightness enhancement

The brightness enhancement is given by the ratio of the brightness of the output surfaces:

$$\frac{B_{3D}}{B_{2D}} = \frac{1-e^{-2\alpha d} R(1-T_{Fresnel})}{1-e^{-2\alpha d}\left[\frac{1-T_{Fresnel}}{r} R + \left(1-\frac{1}{r}\right)R^2\right]} \tag{15}$$

Equation (15) is plotted on Fig. 2 for different values of αd. The curves show that the brightness increases when the aperture is reduced. This is far away from the usual case where the brightness of an emitting surface remains the same even if the surface is apertured. Indeed, brightness enhancement occurs here because of light recycling, the aperture being performed with mirrors

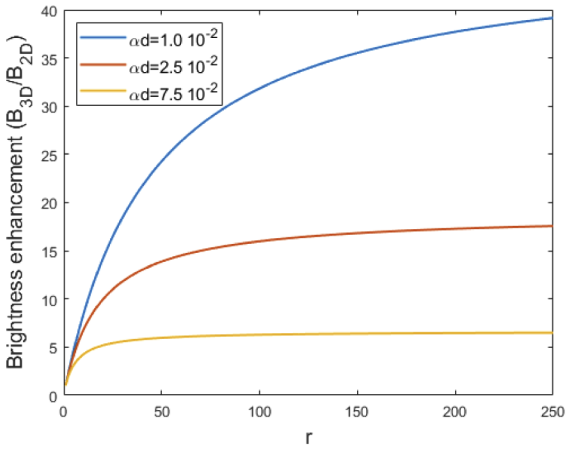

Fig. 2. Theoretical brightness enhancement (from Eq. (15)) versus the aperturing ratio r = S/s for different values of αd, where α is the optical loss coefficient per unit length of the LC and d = d(l) (Eq. (1)). The curves are plotted with a mirror reflectivity R=100% and a Fresnel transmission $T_{Fresnel}$=0.91 corresponding to an interface between Ce:YAG and air.

Optics EXPRESS

in front of an emitting volume. In this volume, light can be recycled by the mirrors on the w×t faces until the rays "find the way out" through the aperture. If the value of αd is low enough, the brightness enhancement can be larger than one order of magnitude.

Figure 2 shows that the brightness enhancement "saturates" versus the aperturing ratio r and tends towards a limit set by Eq. (15) to $\frac{1-e^{-2\alpha d}R(1-T_{Fresnel})}{1-R^2e^{-2\alpha d}}$ showing the importance the mirror reflectivity and the LC losses. This saturation appears when the average propagation length of rays inside the crystal start to be close to the attenuation length (1/ α) : rays with propagation longer than 1/α do not contribute to the output power, being diffused or absorbed before reaching the output.

In the following, the 3D concentration concept is experimentally investigated on a Ce-doped YAG luminescent concentrator.

3. Experimental demonstration with a Ce^{3+}-doped luminescent concentrator

3.1. Experimental setup

The experimental setup is shown on Fig. 3. As LC, we choose a Ce:YAG single-crystal with t=1mm, w=14 mm and l=100 mm (all the dimensions are +/−0.1 mm, faces polished to scratch/dig 60/40 manufactured by Crytur). The Ce:YAG slab has an absorption coefficient of 38 cm^{-1} at 460 nm (corresponding to a Ce^{3+} concentration of 1.2×10^{19} cm^{-3}). YAG crystals have an excellent optical quality and Ce^{3+} ions in YAG present a small overlap between the absorption band (blue) and the emission band (yellow-orange). This leads to a loss coefficient in the order of $10^{-3}cm^{-1}$. The largest dimension of the LC is l=100 mm, close to the limit allowed by the growing process of Ce:YAG. With a mean path length, calculated to be d(l) = 109 mm

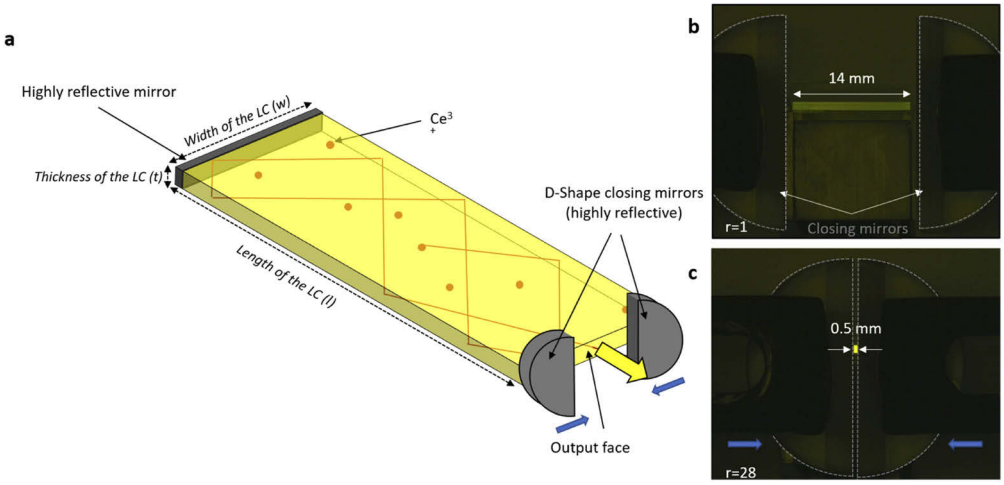

Fig. 3. Illustration of 3D concentration with Ce:YAG. a, Ce:YAG luminescent concentrator. The Ce:YAG dimensions are 1 mm×14 mm×100 mm. The Ce doping concentration is 1.2×10^{19} cm^{-3}. Emission occurs in the yellow-orange. The output surface area s is tuned by the translation of two closing mirrors in front of the output face. b, Picture of the output face with closing mirrors outside of the output surface (r=1). Closing mirrors with a D shape (gray dots). c, Picture of the reduced output surface with translated closing mirrors (r=28), showing a much brighter output face. The signal on the CCD camera coming from the output face is proportional to the brightness and the camera was checked to be linear in the range of detected signals. The LC on the pictures is simply pumped by the surrounding light of the room.

Optics EXPRESS

for θ_{TIR}=33°($n_{Ce:YAG}$=1.83), the product αd is in the order of 10^{-2}. Therefore, we can expect brightness enhancement of one order of magnitude, following Fig. 2.

In this setup, mirrors with a reflectivity of R=99.4% (E02 coating from Thorlabs) are positioned close to the w×t faces. The aperture on the output face can be varied from 14 mm×1mm (r=1) to 0.2 mm ×1mm (r=70) by reducing a slit composed of two mirrors on linear translation stages. The closing mirrors are D-shaped and beveled to avoid as much as possible cutting the light emitted at large angles. Figure 3(b) shows pictures of the output face of the LC taken in two cases: for r=1 and for r=28 when the LC is simply pumped by the surrounding light. Two effects are visible: firstly a qualitative evidence of brightness enhancement, secondly a change of color (from greenish at r=1 to yellowish emission at r=28). To quantify the brightness enhancement, we designed the experiment presented on Fig. 4 where the LC is uniformy illuminated by a multimode blue laser diode at 450 nm emitting 1.6 W. The laser is positioned 20 cm away from the LC such that it illuminates homogeneously the 100×14 mm^2 LC face. We measure the spectral flux with a spectrometer from 520 nm to 680 nm which corresponds to the emission spectrum of the Ce:YAG.

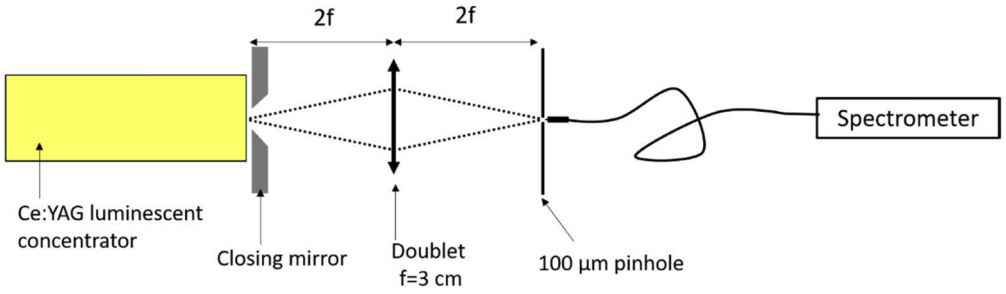

Fig. 4. Experimental setup for spectral brightness measurement (top view). The closing mirrors are beveled to reduce angle limitation at the output of the aperture aperturing. The LC face is imaged using an achromatic doublet in a 2f–2f configuration. The numerical aperture of the optical system is 0.21 (half angle 12°) is designed to be smaller than the aperture of the output beam in the worst case: when the mirrors are very close from one to the other, the aperture is given by the mirror beveling (half angle 24°). A 100-µm-diameter portion at the center of the image is selected with a pinhole and sent to a spectrometer (200–1100 nm AvaSpec-2048 from Avantes).

As concentrators are known to have a Lambertian emission [21] with a constant brightness whatever the output direction, no attention was paid to collect the emitted rays over a broad range of angles. Therefore, a classical doublet in 2f-2f configuration was used. The detection system has a maximum angle of detection of 12°, corresponding to θ_{max}=6.5° inside the crystal and to a mean path length d(l) = 100.3 mm (used for the simulations). Before further investigation, we evaluate the effect of diffraction generated by small apertures created by the closing mirrors on the transmission of the complete optical system. For that, reflections on these mirrors are avoided by inserting a thin dark paper between the mirrors and the LC. The transmission of the optical system is measured as a function of r. For r<50, the transmission remains constant (value T_{max}) and starts to fall down to 96% of T_{max} for r=47, 90% of T_{max} for r=55 and 70% of T_{max} for r=70. This is the reason why we choose a value of r=47 for brightness enhancement measurements reported on Fig. 5.

3.2. Results and analysis

Figure 5(a) shows that the spectral brightness $B_{3D}(\lambda)$ is much higher for r=47 than for r=1. The overall brightness enhancement B_{3D}/B_{2D} is deduced from the Fig. 5(b) by integration of the

Optics EXPRESS

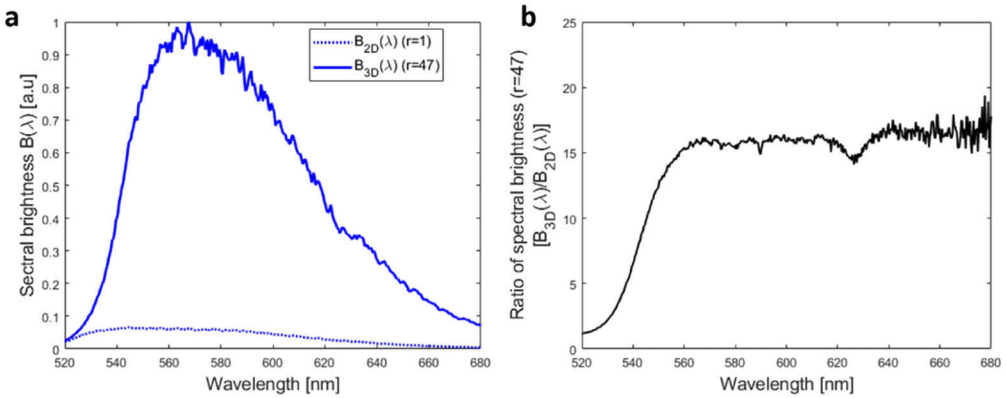

Fig. 5. Measurement of the spectral brightness enhancement of the aperture for r=47. a, Spectral brightness $B_{2D}(\lambda)$ for 2D-concentration (doted blue) and $B_{3D}(\lambda)$ for 3D-concentration at r=47 (plain blue) deduced from measurements by the setup described on Fig. 4. For the measurements, only the size of the aperture changes translating the closing mirrors, all the other optical components are unchanged. b, Spectral brightness enhancement defined as $B_{3D}(\lambda)/B_{2D}(\lambda)$ versus the wavelength.

optical flux over all the emission band. We found a value B_{3D}/B_{2D}=13.5 for a surface ratio r=47. Consequently, a brightness enhancement of more than one order of magnitude is demonstrated with this simple setup. A consequence of the recycling process is a loss of the emitted power when r increases as stated by Eq. (13). When r=47, 29% of the initial power is emitted by the aperture.

Figure 5(b) shows a strong evolution of the ratio $B_{3D}(\lambda)/B_{2D}(\lambda)$. At 520 nm a ratio close to 1 indicates a strong self-absorption limitation on the brightness enhancement process at low wavelengths where absorption and emission spectra overlaps. $B_{3D}(\lambda)/B_{2D}(\lambda)$ increases for longer wavelengths to attain a plateau around 550 nm at a value of 15, where the self-absorption becomes negligible.

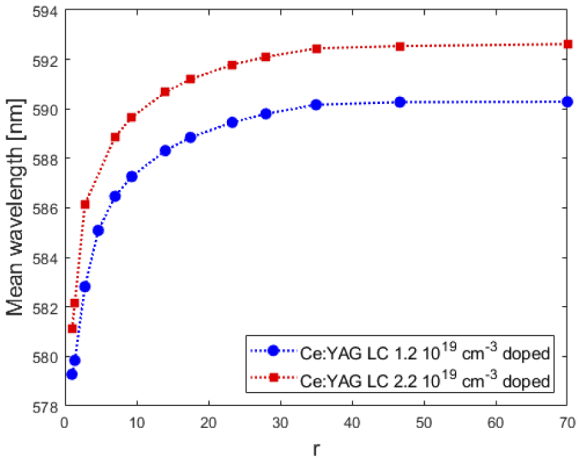

Fig. 6. Mean wavelength of the emission spectrum versus the aperturing ratio for two Ce^{3+} doping concentration of the LC: 1.2×10^{19} cm^{-3} and 2.2×10^{19} cm^{-3}.

Optics EXPRESS

To analyze the change of color more precisely, Fig. 6 gives a plot of the average wavelength versus the aperturing ratio r: the red shift is clearly visible when r increases. This means that the travel distance in the LC increase with r. It can be understood by the probability to go through the aperture at each impact on the output face (1/r). The larger r, the higher the number of bounces to reach the aperture. The red shift variation observes a saturation and remains constant for values of r beyond 20 showing that the emission spectrum has been cleaned from its part subject to reabsorption for long travel distances in the LC. In order to investigate the self-absorption process further, we used a Ce:YAG with a higher doping concentration $n_t=2.2\times10^{19}$ cm^{-3} instead of $n_t=1.2\times10^{19}$ cm^{-3} keeping similar geometrical dimensions. As expected, the average wavelength is more red-shifted at higher Ce^{3+} concentration (Fig. 6).

Figure 7 shows the brightness enhancement for the two Ce:YAG crystals versus the aperturing ratio. The measurement uncertainty is mainly linked to the measurement of aperture size (which causes the uncertainty on the value of r to rise drastically for small apertures). The uncertainty of the position of the mirrors is 10 µm and is linked to the translation stage graduation (horizontal bars on Fig. 7). Correction of diffraction effects have been added for r=47 and r=70.

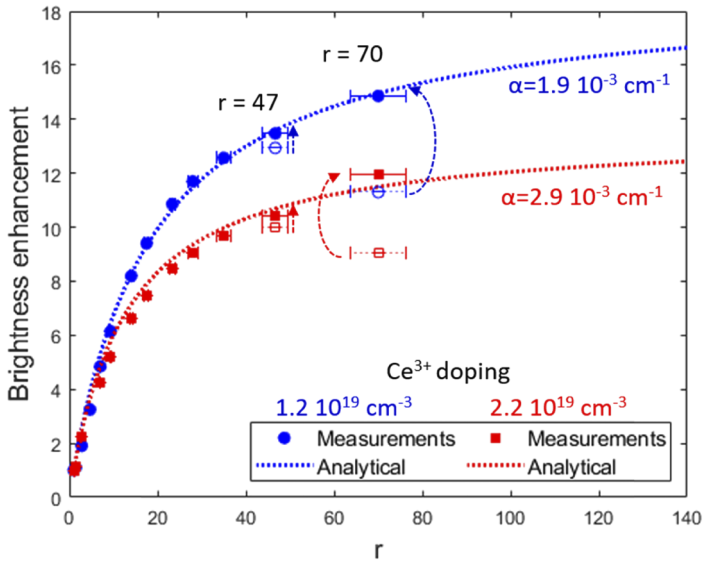

Fig. 7. Brightness enhancement of the aperture of a 3D Ce:YAG LC. The brightness enhancement is given for two Ce:YAG crystals with different doping concentrations. Dots are experimental points and dotted lines are simulations assuming loss coefficients given on the curves. The dashed arrows correspond to the correction of the r=47 and r=70 points (correction of 4% for r=47 and 30% for r=70 according to the measured transmission of the setup). The error bars are linked to the uncertainty of the measurement of the position of the mirrors (10 µm uncertainty on each translation stages).

The experimental curves have the same shape than the theoretical one shown on Fig. 2 inviting us to confront our analytical model with experimental measurement. As opposed to the model described in section 2, the mirrors are not bonded on the w×t faces but positioned very close to the faces, with additional air-Ce:YAG interfaces. In principle, Fresnel reflection should be taken in account for each interface. However, the faces being parallel to the mirrors, those Fresnel reflections contribute also to the light reclycling and induce only a small lateral shift of the beam related to the small distance between the faces and the mirror. Therefore, this effect is not taken in account in the analytical model. In addition, this model does not take into account the wavelength selective reabsorption observed on Fig. 6. The analytical curves are derived in first

Optics EXPRESS

approximation from Eq. (15) with a mean path length d(l) = 100.3 mm related to the numerical aperture of the optical system. The only fitting parameter is the loss coefficient α. It is assumed that α depends linearly on the Ce^{3+} concentration because of absorption ($\alpha=a\times n_t+b$). The slope (Ce^{3+} absorption cross section on the LC emission spectrum) is calculated to be $a=1.0\times10^{22}$ cm^2. The constant is mainly attributed to scattering and is estimated to be $b=0.7\times10^{-3}$ cm^{-1}. Figure 7 shows that the analytical approach gives a good estimation of the experimental brightness enhancement, with loss coefficients α in the 10^{-3} cm^{-1} range corresponding to values expected for high-quality Ce:YAG.

4. Discussion

This work demonstrates theoretically and experimentally that the brightness of a luminescent concentrator can be improved by an additional order of magnitude. The results presented in this paper coupled to the performance of quasi-continuous-wave LC [20] paves the way to a generation of incoherent light sources with brightness at least 200 times higher than LED and with a power of several hundred watts. Hence, 3D-LC have the potential to stand among the brightest incoherent light sources ever designed, filling the gap between high-brightness/limited-power laser sources and high-power/limited-brightness incoherent sources.

The concept of 3D-LC has some opportunities of improvement. Indeed, a large part of the emission is fully trapped inside the LC by total internal reflections (52% in the case of a Ce:YAG (n=1.83) parallelepiped surrounded by air). Trapped rays can be partially extracted by contacting specific optics on the output surface [22,23] or by unpolishing it or by wedging it [21]. To date, all those solutions have been implemented on the entire output face w×t. The next challenge is the extraction of those trapped rays on surfaces s smaller than S = w×t.

Our approach of LED-pumped 3D-LC can bring two main technological improvements for LED-pumped luminescent concentrators. The first one is aperture shaping: in a classical 2D-LC, the output face is rectangular with dimensions w×t. The thickness t being smaller than w, the w/t ratio is often high and can reach 14 [20]. This asymmetric shape requires specific optics such as tapered [17] or cross parabolic optics [18] implemented at the output of the LC to correct the ellipticity. Thanks to the concept developed in this work, the shape of the output aperture can be arbitrary chosen: the only parameter being its surface s, related to the aperturing ratio r = S/s. Hence, it is possible to design a circular output surface adapted to optics with a revolution symmetry and to fiber coupling. The second technological improvement is size shaping of the LC. In a classical 2D-LC, the concentration factor is fundamentally ruled by the geometric ratio (l/t). However, the crystal length is often limited by the growing process (100 mm typically for Ce:YAG which is already a mature crystal). To further increase the concentration factor, one can bond LCs together [16–18]. However, the price to paid is a lower efficiency related to the additional losses of the bond. Another strategy is to reduce the thickness t (0.57 mm has been demonstrated [17]). However, the reduction is limited by mechanical stresses, and by low pump-absorption. It is worth to mention that the width of the LC, w, has no effect on the brightness of a classical 2D-LC. Its only effect is to increase the output power by increasing the area of the pump faces (l×w). Hence, this can explain why the classical LC concentration factor has been capped to 10–20, far away from its thermodynamic limit derived by Eli Yablonovitch in 1980 (generalized brightness theorem [24–26]). Now, the mirrors put on the small faces w×t force the rays to increase their mean path length, as if the LC were longer. In addition, the thickness of the LC can be adapted to the pump absorption quasi-independently of the concentration factor. Moreover, the dimension w has now a role in the concentration factor since it impacts the aperturing ratio (r = w×t/s). For a given aperture a longer width w lead to a higher value of r which induces a higher brightness. Indeed, size shaping and aperture shaping can now be uncoupled: this gives large degrees of freedom for the design.

Optics EXPRESS

More generally, the 3D concentration can be applied to solar harvesting with the interest of a drastic reduction of the number of photovoltaic cells (considering a trade-off with the power loss). It can also be adapted for other emission processes (like thermoluminescence or scintillation).

Funding. Centre National de la Recherche Scientifique (CNRS pre-maturation LEDsGO); Agence Nationale de la Recherche (ANR-10-LABX-0039-PALM).

Acknowledgments. The authors would like to thank the artist Eric Michel for discussions about the work of art called **"**canon à lumière"and Dr Marc Castaing for discussions on luminescent concentrators.

Disclosures. The authors declare no conflicts of interest.

References

1. F. Schütt, M. Zapf, S. Signetti, J. Strobel, H. Krüger, R. Röder, J. Carstensen, N. Wolff, J. Marx, T. Carey, M. Schweichel, M.-I. Terasa, L. Siebert, H.-K. Hong, S. Kaps, B. Fiedler, Y. K. Mishra, Z. Lee, N. M. Pugno, L. Kienle, A. C. Ferrari, F. Torrisi, C. Ronning, and R. Adelung, "Conversionless efficiency and broadband laser light diffusers for high brightness illuminationapplications," Nat. Commun. **11**(1), 1437 (2020).
2. B. Redding, M. A. Choma, and H. Cao, "Speckle-free laser imaging using random laser illumination," Nat. Photonics **6**(6), 355–359 (2012).
3. J. J. Wierer, J. Y. Tsao, and D. S. Sizov, "Comparison between blue lasers and light-emitting diodes for future solid-state lighting," Laser Photonics Rev. **7**(6), 963–993 (2013).
4. L. Fu, "Increasing the brightness of light sources," Dissertation zur Erlangung des Doktorgrades der Naturwissenschaften (Dr. rer. nat.), Fachbereich Physik der Philipps-Universität Marburg (2006).
5. L. Fu, R. Leutz, and H. Ries, "Beating the brightness theorem: thermodynamics of light recycling (experimental)," *Proc. of SPIE 6033, ICO20: Illumination, Radiation, and Color Technologies*, 603304 (2006).
6. A. Malul, D. Nakar, D. Feuermann, and J. M. Gordon, "Effectiveness of recycling light in ultra-bright short-arc discharge lamps," Opt. Express **15**(21), 14194–14201 (2007).
7. O. Ilic, P. Bermel, G. Chen, J. D. Joannopoulos, I. Celanovic, and M. Soljačić, "Tailoring high-temperature radiation and the resurrection of the incandescent source," Nat. Nanotechnol. **11**(4), 320–324 (2016).
8. H. Luo, J. K. Kim, and E. F. Schubert, "Analysis of high-power packages for phosphor-based white light emitting diodes," Appl. Phys. Lett. **86**(24), 243505 (2005).
9. K. Beeson, S. Zimmerman, W. Livesay, R. Ross, C. Livesay, and K. Livesay, "LED-based light-recycling light sources for projection displays," Dig. Tech. Pap. - Soc. Inf. Disp. Int. Symp. **37**(1), 1823–1826 (2006).
10. M. P. C. M. Krijn, B. A. Salters, and O. H. Willemsen, "LED-based mini-projectors," Proc. SPIE **6196**, 619602 (2006).
11. W. H. Weber and J. Lambe, "Luminescent greenhouse collector for solar radiation," Appl. Opt. **15**(10), 2299–2300 (1976).
12. N. Giebink, G. Wiederrecht, and M. Wasielewski, "Resonance-shifting to circumvent self-absorption loss in luminescent solar concentrators," Nat. Photonics **5**(11), 694–701 (2011).
13. F. Meinardi, A. Colombo, K. A. Velizhanin, R. Simonutti, M. Lorenzon, L. Beverina, R. Viswanatha, V. I. Klimov, and S. Brovelli, "Large-area luminescent solar concentrators based on 'Stokes-shift-engineered' nanocrystals in a mass-polymerized PMMA matrix," Nat. Photonics **8**(5), 392–399 (2014).
14. F. Meinardi, H. McDaniel, F. Carulli, A. Colombo, K. A. Velizhanin, N. S. Makarov, R. Simonutti, V. I. Klimov, and S. Brovelli, "Highly efficient large-area colourless luminescent solar concentrators using heavy-metal-free colloidal quantum dots," Nat. Nanotechnol. **10**(10), 878–885 (2015).
15. F. Meinardi, S. Ehrenberg, L. Dhamo, F. Carulli, M. Mauri, F. Bruni, R. Simonutti, U. Kortshagen, and S. Brovelli, "Highly efficient luminescent solar concentrators based on earth-abundant indirect-bandgap silicon quantum dots," Nat. Photonics **11**(3), 177–185 (2017).
16. A. Barbet, A. Paul, T. Gallinelli, F. Balembois, J.-P. Blanchot, S. Forget, S. Chénais, F. Druon, and P. Georges, "Light-emitting diode pumped luminescent concentrators : a new opportunity for low-cost solid-state lasers," Optica **3**(5), 465–468 (2016).
17. J. Sathian, J. D. Breeze, B. Richards, N. M. Alford, and M. Oxborrow, "Solid-state source of intense yellow light based on a Ce:YAG luminescent concentrator," Opt. Express **25**(12), 13714–13727 (2017).
18. D. K. G. de Boer, D. Bruls, and H. Jagt, "High-brightness source based on luminescent concentration," Opt. Express **24**(14), A1069–1074 (2016).
19. D. K. G. de Boer and L. Haenen, "Extraction optics for high lumen density sources," J. Eur. Opt. Soc.-Rapid Publ. **15**(1), 8 (2019).
20. P. Pichon, A. Barbet, J.-P. Blanchot, F. Druon, F. Balembois, and P. Georges, "Light-emitting diodes, a new paradigm for Ti:sapphire pumping," Optica **5**(10), 1236–1239 (2018).
21. T. Gallinelli, A. Barbet, F. Druon, F. Balembois, P. Georges, T. Billeton, S. Chenais, and S. Forget, "Enhancing brightness of Lambertian light sources with luminescent concentrators: the light extraction issue," Opt. Express **27**(8), 11830–11843 (2019).
22. S. Roelandt, Y. Meuret, D. K. G. de Boer, D. Bruls, P. Van De Voorde, and H. Thienpont, "Incoupling and outcoupling of light from a luminescent rod using a compound parabolic concentrator," Opt. Eng. **54**(5), 055101 (2015).

Optics EXPRESS

23. P. Pichon, J.-P. Blanchot, F. Balembois, and P. Georges, "New LED-based high-brightness incoherent light source in the SWIR," Opt. Express **26**(7), 9353–9362 (2018).
24. E. Yablonovitch, "Thermodynamics of the fluorescent planar concentrator," J. Opt. Soc. Am. **70**(11), 1362–1363 (1980).
25. G. Smestad, H. Ries, R. Winston, and E. Yablonovitch, "The thermodynamic limits of light concentrators," Sol. Energy Mater. **21**(2-3), 99–111 (1990).
26. I. Papakonstantinou and C. Tummeltshammer, "Fundamental limits of concentration in luminescent solar concentrators revised: the effect of self-absorption and nonunity quantum yield," Optica **2**(10), 841–849 (2015).